Faraday Discussions

Accepted Manuscript

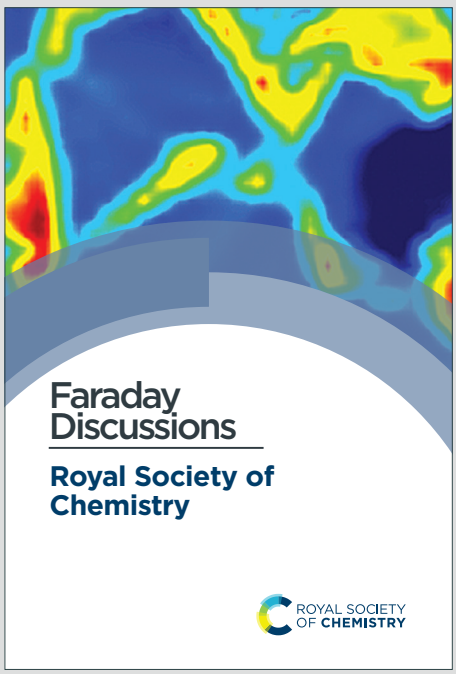

This article can be cited before page numbers have been issued, to do this please use: T. Yamamoto, T. Ozawa, M. Tomisaki and Y. Einaga, *Faraday Discuss.*, 2026, DOI: 10.1039/D6FD00071A.

ROYAL SOCIETY OF CHEMISTRY

www.rsc.org/faraday_d

Faraday Discussions

View Article Online
DOI: 10.1039/D6FD00071A

PAPER

Interfacial engineering for redirecting CO_2 electroreduction selectivity on boron-doped diamond: from formic acid to carbon monoxide

Takashi Yamamoto,*[a] Taiga Ozawa,[a] Mai Tomisaki[b] and Yasuaki Einaga*[a]

[a]*Department of Chemistry, Keio University, Yokohama 223-8522, Japan. E-mail: takyama@chem.keio.ac.jp (T.Y.); einaga@keio.jp (Y.E.)*
[b]*International Institute for Carbon-Neutral Energy Research (WPI-I2CNER), Kyushu University, Fukuoka 819-0395, Japan.*

Received 00th January 20xx, Accepted 00th January 20xx
DOI: 10.1039/x0xx00000x

The electrochemical carbon dioxide reduction reaction (eCO_2RR) on boron-doped diamond (BDD) electrodes predominantly yields formic acid (HCOOH) as the primary product. Redirecting the reaction pathway toward highly valuable carbon monoxide (CO) remains a significant challenge due to the chemical inertness of the BDD surface. Herein, we present an interfacial engineering strategy to tune the product selectivity from HCOOH to CO on BDD electrodes. First, functionalisation of the BDD surface with nitrogen-containing molecules such as aniline and pyrazole effectively captured CO_2, successfully directing the reaction pathway toward CO, and established molecular modification as a proof of concept for redirecting selectivity. Second, utilising an aqueous $KClO_4$ electrolyte dynamically facilitated CO production by minimising specific anion adsorption, providing a considerably more facile and practical route to the same selectivity switch. Through systematic optimisation of the eCO_2RR conditions in 0.1 M $KClO_4$, we achieved a maximum Faradaic efficiency for CO production (FE_{CO}) of 72% at an applied potential of −1.9 V (*vs.* Ag/AgCl; −1.46 V *vs.* RHE), an electrolyte flow rate of 500 mL min^{-1}, and an operating temperature of 5 °C. Electrochemical analyses revealed that increasing the flow rate enhanced the CO_2 supply by significantly reducing the diffusion layer thickness. Moreover, decreasing the temperature not only increased CO_2 solubility but also selectively suppressed the competing hydrogen evolution reaction (HER). Temperature-dependent linear sweep voltammetry experiments further revealed that this suppression is driven primarily by a negative shift of the HER onset potential rather than by any appreciable shift of the CO_2 reduction onset. These findings provide fundamental insights into the reaction mechanisms on inert sp^3-carbon surfaces and demonstrate that interfacial engineering is an effective strategy for developing selective CO2 conversion systems on BDD, although practical implementation will require further advances in electrode fabrication, operating conditions, and energy efficiency.

Introduction

Converting carbon dioxide (CO_2) into value-added chemical feedstocks and fuels is a pivotal challenge for establishing a sustainable, carbon-neutral society.[1] In the context of carbon capture, utilisation, and storage, a variety of catalytic approaches for CO_2 conversion have been extensively investigated, including organic,[2] photochemical,[3] and electrochemical processes.[4] Among these, the electrochemical CO_2 reduction reaction (eCO_2RR) has garnered significant attention as a particularly promising pathway. The eCO_2RR offers several distinct advantages: (i) the process can be directly driven by electricity derived from renewable energy sources, thereby enabling carbon recycling; (ii) the reaction proceeds under mild operational conditions, specifically at ambient temperature and pressure; and (iii) the product selectivity and catalytic activity can be effectively modulated by finely tuning key parameters, such as the nature of the electrode materials, the composition of the electrolytes, and the applied potentials.

While various reduction products can be generated via the eCO_2RR, carbon monoxide (CO) stands out as a particularly versatile and high-value target.[5] CO is a fundamental building block in the chemical industry, most notably as a key constituent of synthesis gas (syngas) when

View Article Online
DOI: 10.1039/D6FD00071A

mixed with hydrogen (H_2). Syngas serves as a key feedstock for the Fischer–Tropsch process, a well-established industrial technology for producing a wide range of synthetic fuels.[6] Therefore, achieving highly selective CO production via the eCO_2RR is not only scientifically intriguing but also offers a critical pathway for the sustainable synthesis of essential chemical commodities and liquid energy carriers.[7]

Among various electrode materials, boron-doped diamond (BDD) has emerged as a superior platform for the eCO_2RR due to its exceptional physical and chemical stability, coupled with an exceptionally wide potential window.[8] Crucially, BDD exhibits a high overpotential for proton reduction, which effectively suppresses the competitive hydrogen evolution reaction (HER) in aqueous solutions, thereby providing an ideal environment for efficient CO_2 reduction. In our previous studies, we have demonstrated the outstanding utility of BDD electrodes for the highly efficient and stable production of formic acid (HCOOH) via the eCO_2RR, achieving an excellent Faradaic efficiency (FE) of up to 95% via the eCO_2RR.[9] Despite these remarkable achievements, HCOOH remains the predominant product on unmodified BDD electrodes. Since CO is highly significant as a versatile building block, redirecting the reaction pathway from HCOOH to CO on BDD is highly desirable. However, this presents a formidable challenge; because the sp^3-bonded carbon surface of BDD is chemically inert, it is difficult to strongly bind and stabilize the reaction intermediates required for CO evolution. Consequently, modulating its intrinsic product selectivity requires innovative strategies. Such modulation is particularly pertinent in light of the power-to-X (PtX) paradigm,[10] in which the selective electrochemical conversion of CO_2 to CO is positioned as a key step for coupling renewable electricity to established industrial value chains. In this framework, electrochemically produced CO serves as a syngas component that can be upgraded to liquid fuels and chemicals via established Fischer–Tropsch and methanol synthesis.[6,11,12] From this standpoint, BDD's precious-metal-free composition and its demonstrated operational stability in corrosive aqueous environments[8] make it a potentially attractive platform for sustainable applications, although practical deployment will need to account for the cost and scalability of CVD-based electrode fabrication. Realising this potential, however, requires that its intrinsic selectivity be rationally redirected toward CO.

Herein, we present an interfacial engineering strategy to redirect the eCO_2RR pathway on BDD electrodes, shifting the primary product from HCOOH to CO. To overcome the intrinsic inertness of the BDD surface, we built on two independent approaches focused on modulating the local environment at the electrode-electrolyte interface. In our previous studies, we demonstrated the functionalisation of the BDD surface with nitrogen-containing molecules, such as aniline[13] and pyrazole,[14] effectively captures CO_2 and redirects the reaction pathway toward CO, achieving up to a 16-fold increase in the FE ratio of CO to HCOOH. While these results establish molecular modification as a viable proof of concept, the multi-step surface preparation involved limits its practicality for large-scale applications. This recognition motivates the second approach investigated here, namely electrolyte engineering using aqueous $KClO_4$ solution, in which the weakly adsorbing perchlorate anion preserves a CO_2-rich interfacial microenvironment and achieves the same selectivity switch through a considerably more facile route. Building on the initial observation of this selectivity switch reported previously,[15] the present work provides, for the first time, a full parametric optimisation across applied potential, electrolyte flow rate, and operating temperature, ultimately achieving a maximum FE of CO production of 72%. Electrochemical analysis further reveals mechanistic features specific to BDD that are qualitatively distinct from those reported on metallic catalysts, providing new insights into the eCO_2RR on sp^3-carbon surfaces.

Methods

General information

All reagents were commercially available and used without further purification. Ultrapure water (18.2 MΩ · cm at 25 °C) was supplied by a DIRECT-Q 3 UV system (Millipore). A boron-doped diamond (BDD) electrode with a boron concentration of 1% was prepared on a Si substrate using a microwave plasma chemical vapor deposition (MPCVD) system (AX5250M, Cornes Technologies) according to the previously reported procedures.[16] The prepared electrode was characterized using an Acton SP2500 Raman spectrometer (Princeton Instruments) (Fig. S1).

Electrochemical CO_2 reduction reactions (eCO_2RR)

The BDD electrodes were pretreated by immersion in aqua regia for 30 min, followed by UV-ozone oxidation using a low-pressure mercury lamp (UVB40; Sen Lights Corp.) for 30 min, as described in our previous work.[17]

A two-compartment polytetrafluoroethylene (PTFE) flow cell[9] was used for the eCO_2RR (Fig. S2). The compartments were separated by a Nafion membrane (NRE-212; Sigma-Aldrich). The prepared 1% BDD, a Pt plate, and an Ag/AgCl (3 M NaCl) electrode were used for the working, counter, and reference electrodes, respectively. The geometric areas of the working and counter electrodes in this cell were both 9.62 cm^2. An aqueous $KClO_4$ solution was used as the electrolyte. The volumes of the catholyte and anolyte were 50 mL each. The temperature of the electrolytes was controlled using a low-temperature circulator (CCA-1112A; EYELA).

Prior to the eCO_2RR, N_2 gas was bubbled into the catholyte for 30 min at a flow rate of 200 mL min^{-1} to remove the dissolved oxygen, after which CO_2 gas was bubbled for 15 min at a flow rate of 250 mL min^{-1}. During the eCO_2RR, CO_2 gas was bubbled at a flow rate of less than 25 mL min^{-1} and the electrolytes were circulated. Electrolysis was carried out at constant potential using a potentiostat/galvanostat system (PGSTAT204; Metrohm Autolab) until the total charge had reached 69 C. After electrolysis, N_2 gas (50 mL min^{-1}) was bubbled for 15 min to collect the gas products.

View Article Online
DOI: 10.1039/D6FD00071A

The products obtained from the eCO_2RR were quantified using a high-performance liquid chromatography (HPLC) system equipped with an electroconductivity detector or a UV-visible detector (Prominence; Shimadzu Corporation), and a gas chromatography (GC) system equipped with a thermal conductivity detector or a flame ionisation detector (GC-2014; Shimadzu Corporation). Further details regarding the product analysis are provided in our previous paper.[17] Briefly, liquid-phase products (primarily HCOOH) remaining in the catholyte after electrolysis were quantified by HPLC, whereas gaseous products (CO and H_2) collected in the N_2-purge stream were quantified by GC using thermal conductivity and flame ionisation detectors, respectively. Product amounts were determined from external calibration curves constructed from authentic standards, and the Faradaic efficiencies reported below represent the average of independently repeated measurements. The Faradaic efficiency (FE) was calculated using the following equation, FE (%) = nFc / Q × 100, where n is the number of electrons required to generate the products from CO_2, F is the Faraday constant (96,485 C mol^{-1}), c is the amount of the product (mol), and Q is the total charge passed (69 C).

Electrochemical measurements

Electrochemical measurements were performed using the PGSTAT204 potentiostat. Cyclic voltammetry (CV) and chronoamperometry (CA) measurements were conducted to estimate the diffusion layer thickness. CV measurements were carried out in a 0.01 M $K_3[Fe(CN)_6]$ aqueous solution (pH 6.9) over a potential range of 1.2 to –1.2 V (*vs.* Ag/AgCl) at a scan rate of 50 mV s^{-1}. CA measurements were performed in a 0.01 M $K_3[Fe(CN)_6]$ aqueous solution (pH 6.9) at –0.2 V (*vs.* Ag/AgCl) for 120 s. Temperature-dependent linear sweep voltammetry (LSV) measurements were conducted in a CO_2-saturated 0.1 M $KClO_4$ aqueous solution over a potential range of 0.5 to –2.5 V (*vs.* Ag/AgCl) at a scan rate of 50 mV s^{-1}. All potentials are reported versus Ag/AgCl (3 M NaCl) and converted to the RHE scale using E (*vs.* RHE) = E (*vs.* Ag/AgCl) + 0.209 + 0.0592 × pH, where the bulk pH of the 0.1 M $KClO_4$ aqueous solution was 3.89 before electrolysis. We note that the post-electrolysis pH was not measured; the RHE conversion is therefore based on the pre-electrolysis value. No correction for the temperature dependence of either the Ag/AgCl reference electrode potential or the RHE conversion factor, RT / F × ln(10), was applied in the present study. The temperature coefficient of the Ag/AgCl (3 M NaCl) electrode is approximately −0.4 to −0.8 mV °C^{-1} depending on the exact composition of the internal filling solution.[18] Adopting the upper bound of this range, the maximum potential offset across the temperature range investigated (5–30 °C) corresponds to a change of approximately 18 mV. The variation in the RHE conversion factor across the same range corresponds to a change of approximately 15 mV in the pH-dependent term. Both effects are small relative to the large potential shifts observed for the HER onset across this temperature range, consistent with previous eCO_2RR studies that have likewise found the temperature dependence of Ag/AgCl reference electrodes to be negligible within this range.[19] The conclusions regarding the contrasting temperature sensitivity of the two competing reactions are not affected by these uncorrected offsets.

Results and Discussion

Electrochemical CO_2 reduction reactions (eCO_2RR) using molecularly modified boron-doped diamond (BDD) electrodes

It is well established that the product selectivity in the eCO_2RR strongly depends on the adsorption properties of the reaction intermediates on the electrode (catalyst) surface.[12,20] Therefore, tuning these properties should enable the rational control of product selectivity, even when utilising the same underlying electrode material. The present work builds on two approaches to modulating the local environment at the electrode–electrolyte interface. We first examine the functionalisation of the BDD surface with nitrogen-containing molecules as a proof-of-concept demonstration that surface modification can redirect selectivity from HCOOH to CO. Since nitrogen-containing compounds are known to capture CO_2, we modified the BDD surface with (i) aniline (AN)[13] and (ii) pyrazole (PZ)[14] via electrografting reactions and their product selectivity in the eCO_2RR (Fig. 1). These molecular modification results are presented here to establish the conceptual foundation and to motivate the subsequent development of a more practical electrolyte engineering approach using $KClO_4$ aqueous solution, which constitutes the primary focus of the present study.

For the AN-modified BDD (AN-BDD) electrode, linear sweep voltammetry (LSV) measurements revealed a positive shift in the CO_2 reduction potential. This shift is presumably attributed to the enhanced electrophilicity of the carbon atom in CO_2 upon the capture by the surface-anchored AN molecules. To further elucidate this mechanism, potential-dependent *in situ* attenuated total reflection infrared (ATR-IR) spectroscopy was performed. The results revealed the formation of a carbamate intermediate between the surface AN and CO_2 at potentials more negative than the CO_2 reduction potential. Consequently, CO production became dominant during the eCO_2RR, and the ratio of Faradaic efficiencies (FE_{CO} / FE_{HCOOH}), a key indicator of product selectivity, was enhanced by up to a factor of 8 compared to the unmodified BDD (Bare-BDD).

Similarly, for the PZ-modified BDD (PZ-BDD), LSV measurements confirmed a positive shift in the CO_2 reduction potential. In the eCO_2RR, CO generation was further favored, and the FE_{CO} / FE_{HCOOH} ratio increased up to twofold compared to that of the AN-BDD. This pronounced enhancement is likely because one of the two nitrogen atoms in the pyrazole ring captures CO_2 via a nucleophilic attack, while the adjacent N–H group forms an intramolecular hydrogen bond with the captured CO_2. This synergistic interaction results in strong CO_2 capture and the formation of a highly stabilized intermediate.

Although the functionalisation with these molecules successfully improved the CO production selectivity on BDD electrodes during the eCO_2RR, developing a more facile and practical strategy remains essential for industrial applications. We have previously reported that the primary product dynamically shifts from HCOOH to CO when $KClO_4$ is employed as the supporting electrolyte.[15] Therefore, we subsequently conducted a detailed optimisation of the eCO_2RR conditions in an aqueous $KClO_4$ solution using unmodified BDD electrodes.

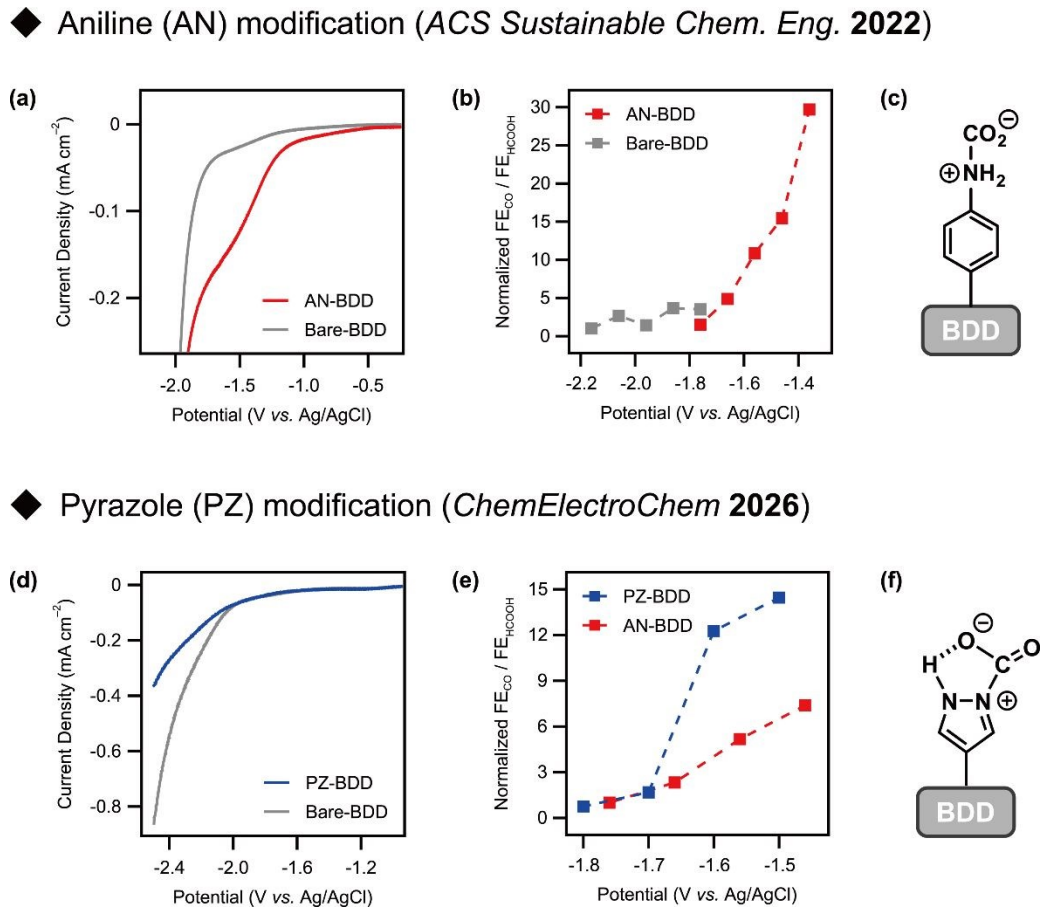

Fig. 1 eCO_2RR on molecularly modified BDD electrodes: (top) aniline (AN) modification and (bottom) pyrazole (PZ) modification. (a, d) Linear sweep voltammograms. (b, e) Relationships between the selectivity for CO production and the applied potential. (c, f) Schematic illustrations of CO_2 capture by the surface molecules.

State-of-the-art CO_2-to-CO electrocatalysts, most notably Au and Ag, are known to reach Faradaic efficiencies exceeding 90% in flow cells and gas-diffusion electrode configurations.[21] Compared with such metallic benchmarks, the efficiencies achieved on BDD in this work are not intended to compete in terms of geometric current density alone. Rather, BDD offers a distinct and complementary value proposition that is particularly pertinent to the sustainable chemistry of electrofuels. First, BDD is a metal-free electrode based on earth-abundant elements that does not rely on precious or critical metals, which is expected to decouple large-scale deployment of the eCO_2RR from supply-chain risks associated with Au- or Ag-based catalysts. Second, its chemical robustness and wide potential window are highly beneficial under the dynamic operation at high overpotentials that intermittent renewable power sources impose on PtX electrolysers, where metallic catalysts are often prone to restructuring, dissolution, or poisoning.[21] Third, the very inertness that limits intrinsic CO selectivity also renders BDD an unusually "clean" platform on which the interfacial microenvironment can be tuned. Such tuning can be achieved through surface functionalisation and electrolyte engineering, without interference from strong intrinsic binding of reaction intermediates.[4] Within this framing, the ability to reversibly switch selectivity between HCOOH and CO on the same electrode is itself a useful property: it opens the possibility of adjusting the output of a BDD-based electrolyser between a liquid carbon carrier (HCOOH, of interest for hydrogen storage)[12] and a syngas component (CO) in response to downstream demand, a flexibility that is difficult to realise with metallic catalysts optimised for a single product.

Optimisation of the applied potential

View Article Online
DOI: 10.1039/D6FD00071A

First, we investigated the optimal applied potential to maximize CO production. The eCO_2RR was conducted by varying the applied potential from −2.4 to −1.6 V (*vs.* Ag/AgCl; −1.96 to −1.16 *vs.* RHE). During these measurements, the electrolyte (0.1 M $KClO_4$ aqueous solution), flow rate (100 mL min^{-1}), and operating temperature (room temperature, 22 °C) were kept constant (Fig. 2). At more negative potentials, the competing hydrogen evolution reaction (HER) became dominant, whereas at more positive potentials, the eCO_2RR did not proceed sufficiently. Specifically, the Faradaic efficiency for CO production (FE_{CO}) reached its maximum value of 53% at −1.9 V (*vs.* Ag/AgCl; −1.46 V *vs.* RHE). Consequently, the applied potential was fixed at −1.9 V (*vs.* Ag/AgCl; −1.46 V *vs.* RHE) for all subsequent parameter optimisation studies. Additionally, the effect of the electrolyte concentration was briefly examined at 0.05, 0.075, and 0.1 M, with 0.1 M being identified as the optimal concentration for achieving the highest FE_{CO}. Therefore, 0.1 M was employed in all following experiments.

The volcano-shaped dependence of FE_{CO} on applied potential reflects the superposition of two competing regimes. At potentials more positive than approximately –1.9 V *vs.* Ag/AgCl (−1.46 V *vs.* RHE), the driving force for CO_2 activation on the inert sp^3-carbon surface is insufficient, and the overall current density remains low. As a result, FE_{CO} is limited by the slow kinetics of CO formation rather than by the availability of CO_2. At more negative potentials, the interfacial concentration of dissolved CO_2 becomes depleted by the increasing cathodic current, and the competing HER progressively takes over as the dominant cathodic process, driving FE_{CO} back down. The optimum at −1.9 V *vs.* Ag/AgCl (−1.46 V *vs.* RHE) therefore marks the potential at which these two limitations balance most favourably on the unmodified BDD surface, and it is also the potential at which subsequent investigations of mass transport (flow rate) and temperature can most meaningfully probe the competition between eCO_2RR and HER.

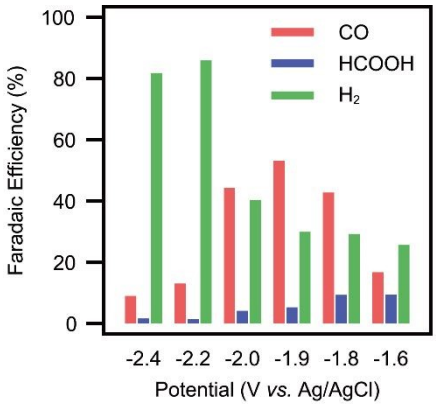

Potential (V *vs.* RHE)	Faradaic Efficiencies (%)		
	CO	HCOOH	H_2
−1.96	9	2	82
−1.76	13	1	86
−1.56	44	4	40
−1.46	53	5	30
−1.36	43	9	29
−1.16	17	9	26

Fig. 2 Potential dependence on the Faradaic efficiencies (FEs) for the eCO_2RR products. Conditions: 0.1 M $KClO_4$ aqueous solution, electrolyte flow rate of 100 mL min^{-1}, and operating temperature of 22 °C.

Optimisation of the flow rate

Next, we investigated the effect of the electrolyte flow rate on CO production. The eCO_2RR was conducted by varying the flow rate from 100 to 600 mL min^{-1}. During these measurements, the applied potential (−1.46 V *vs.* RHE), the electrolyte concentration (0.1 M $KClO_4$ aqueous solution), and the operating temperature (room temperature, 22 °C) were kept constant (Fig. 3). As the flow rate increased, the Faradaic efficiencies for both CO and HCOOH production improved, while the competing hydrogen evolution reaction (HER) was suppressed. Notably, the FE_{CO} reached a maximum of 71% at a flow rate of 500 mL min^{-1}. This enhancement is likely attributed to the increased supply of CO_2 to the vicinity of the BDD electrode, driven by forced convection at higher flow rates.

View Article Online
DOI: 10.1039/D6FD00071A

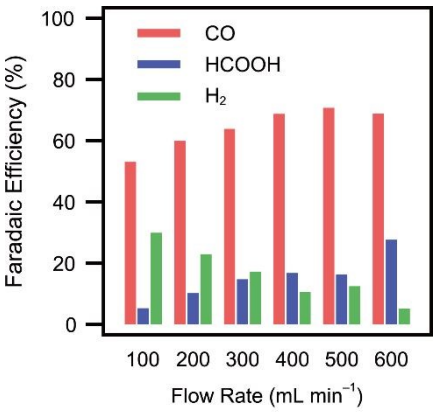

Flow Rate (mL min^{-1})	Faradaic Efficiencies (%)		
	CO	HCOOH	H_2
100	53	5	30
200	60	10	23
300	63	15	17
400	69	17	11
500	71	16	12
600	69	28	5

Fig. 3 Flow rate dependence on the FEs for the eCO_2RR products. Conditions: applied potential of −1.46 V (*vs.* RHE), 0.1 M $KClO_4$ aqueous solution, and operating temperature of 22 °C.

We hypothesized that the enhanced CO_2 supply was attributed to a decrease in the diffusion layer thickness near the electrode surface. To verify this, we estimated the diffusion layer thickness from the mass-transport-limited current density obtained via electrochemical measurements.[22] First, cyclic voltammetry (CV) was performed in a 0.01 M $K_3[Fe(CN)_6]$ aqueous solution (pH 6.9) at various flow rates ranging from 100 to 600 mL min^{-1} (Fig. 4a). The potential at which the current density reached a plateau was defined as the potential yielding the mass-transport-limited current density. Because the current density stabilized at potentials more negative than −0.2 V (*vs.* Ag/AgCl), we subsequently conducted chronoamperometry at an applied potential of −0.2 V (*vs.* Ag/AgCl). These measurements were carried out for 120 s, and the average current density over the final 20 s (*i.e.*, from 100 to 120 s) was calculated and defined as the mass-transport-limited current density.

Based on the mass-transport-limited current density obtained above, the diffusion layer thickness was estimated using the following procedure. Fick's first law is expressed as follows:

$$J = -D\frac{\partial\varphi}{\partial x} (1)$$

where J is the flux, D is the diffusion coefficient, and $\partial\varphi / \partial x$ represents the concentration gradient. By defining the diffusion layer thickness, δ, as the distance over which the concentration changes from the surface to the bulk concentration (φ_0), the steady-state flux (J_{ss}) can be approximated as:

$$J_{ss} = D\frac{\varphi_0}{\delta} (2)$$

The relationship between the magnitude of steady-state current density (j_{ss}) and the flux under mass-transport-limited conditions is given by:

$$|j_{ss}| = nFJ_{ss} (3)$$

where n is the number of electrons transferred and F is the Faraday constant (96485 C mol^{-1}). By combining Equations (2) and (3), δ can be expressed as:

$$\delta = D\frac{\varphi_0 nF}{|j_{ss}|} (4)$$

Using the diffusion coefficient (D) of $K_3[Fe(CN)_6]$ and the number of electrons transferred (n), the relationship between the flow rate and the diffusion layer thickness (δ) was determined (Fig. 4c). As expected, δ clearly decreased with increasing flow rate. It should be noted, however, that the chronoamperometric measurements using $[Fe(CN)_6]^{3-}$ as a redox probe were conducted under conditions that differ from those of the productive eCO_2RR experiments in terms of electrolyte composition, CO_2 saturation, and operating temperature. The estimated δ values therefore serve as a hydrodynamic proxy and should not be taken as a direct measure of the CO_2 concentration profile at the reacting BDD interface. The numerical δ values obtained at each flow rate, together

with repeatability data, are provided in Table S4. This result confirms that the hydrodynamic mass-transport regime is substantially altered by the flow rate and, in turn, supports the interpretation that the enhancement of the eCO_2RR at higher flow rates is driven by improved CO2 supply resulting from the reduction in the diffusion layer thickness.

View Article Online
DOI: 10.1039/D6FD00071A

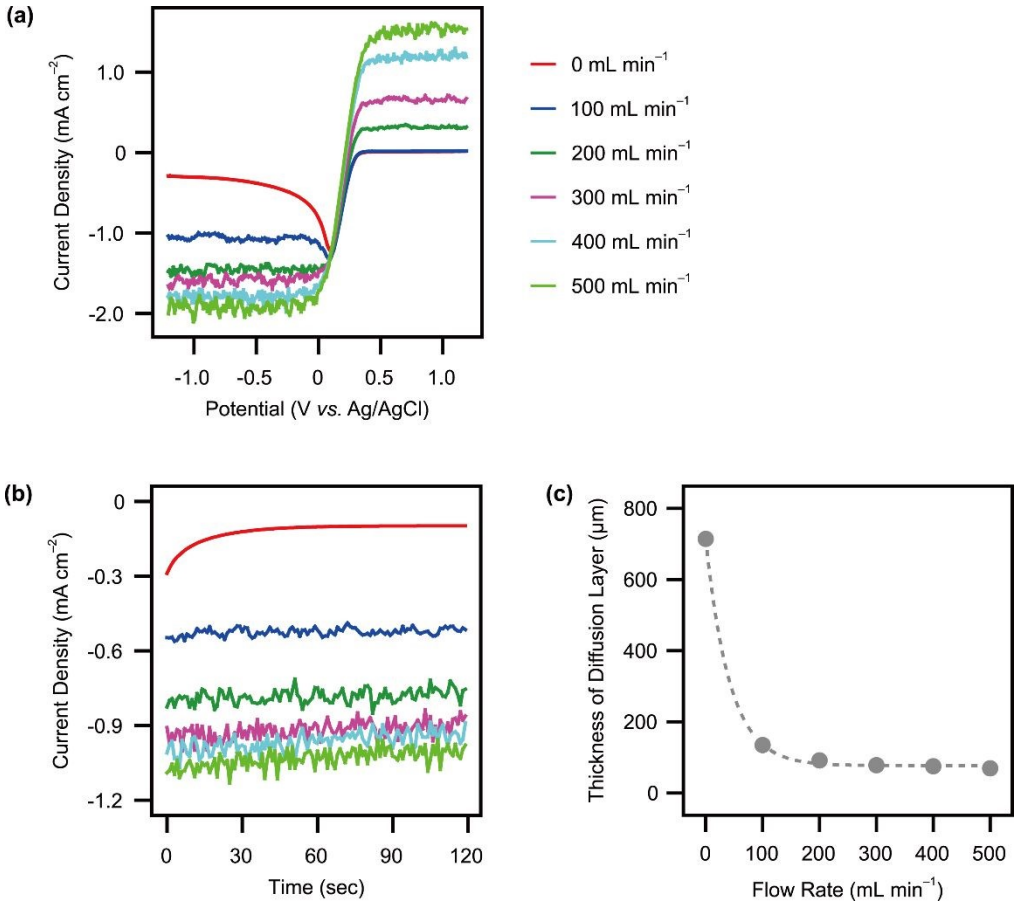

Fig. 4 Electrochemical estimation of the diffusion layer thickness in a 0.01 M $K_3[Fe(CN)_6]$ aqueous solution (pH 6.9). (a) Cyclic voltammograms at various flow rates (potential range: 1.2 to –1.2 V (*vs.* Ag/AgCl); scan rate of 50 mV s^{-1}). (b) Chronoamperograms at –0.2 V (*vs.* Ag/AgCl) for 120 s at various flow rates. (c) Relationships between the calculated diffusion layer thickness (δ) and the electrolyte flow rate. All measurements were performed at 22 °C, and the data points represent the mean of three independent measurements (see Table S4 for repeatability data).

Optimisation of the temperature of electrolytes

Next, we investigated the effect of the electrolyte temperature on CO production. The eCO_2RR was conducted by varying the temperature from 0 to 30 °C, while keeping the applied potential (−1.46 V *vs.* RHE), the electrolyte concentration (0.1 M $KClO_4$), and the flow rate (500 mL min^{-1}) constant (Fig. 5). The electrolyte temperature was precisely controlled using a low-temperature circulator. The Faradaic efficiency for CO production (FE_{CO}) increased as the temperature decreased, reaching a plateau of 72% at 13 °C and below. This enhancement is likely due to the increased solubility of CO_2 at lower temperatures,[23,24] which increases the concentration of CO_2 available for reaction at the BDD electrode surface.

Furthermore, the HER was significantly suppressed at lower temperatures. It has been reported that the onset potential for HER shifts to more negative values as the temperature decreases.[25] Rodriguez et al. previously investigated the temperature dependence of the eCO_2RR on Au electrodes in CO_2-saturated $Mg(ClO_4)_2$ solution; they reported that lower temperatures not only shift the HER potential negatively but also shift the CO_2 reduction potential positively, thereby enhancing selectivity.[26] To clarify the mechanism on BDD, we performed LSV measurements in CO_2-saturated $KClO_4$ aqueous solutions. We note that the onset potentials defined here are operationally determined as the potentials where the current densities reached −0.05 and −0.025 mA cm^{-2} for the HER and CO_2 reduction, respectively. These thresholds were selected as values clearly distinguishable from the baseline current while remaining within the kinetic-controlled region of each LSV curve, and were applied uniformly across all temperatures so that comparisons between conditions reflect relative shifts in onset potential rather than the choice of threshold. The reported onset potentials should therefore be interpreted accordingly. Furthermore, no correction for the temperature

View Article Online
DOI: 10.1039/D6FD00071A

dependence of the Ag/AgCl reference electrode potential was applied in the present study. The maximum uncertainty in the reported onset potentials arising from this uncorrected offset is approximately 18 mV across the temperature range investigated, which is small relative to the substantially larger magnitude of the observed HER onset shift and does not affect the conclusions regarding the contrasting temperature sensitivity of the two competing reactions. The results showed that the HER onset potential shifted significantly in the negative direction at lower temperatures, whereas the CO_2 reduction onset potential remained essentially unchanged. This contrasting temperature sensitivity of the two competing reactions is consistent with HER suppression playing a significant role in the observed improvement in FE_{CO} at lower temperatures.

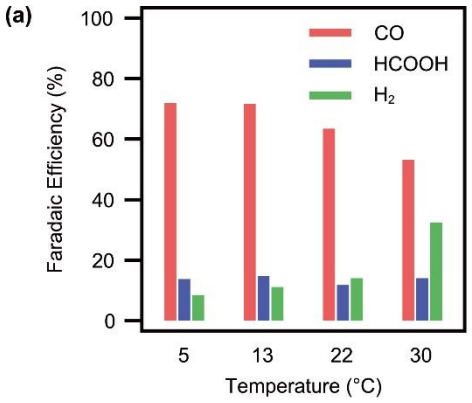

Temperature (°C)	Faradaic Efficiencies (%)		
	CO	HCOOH	H_2
5	72	14	8
13	72	15	24
22	63	12	14
30	53	14	32

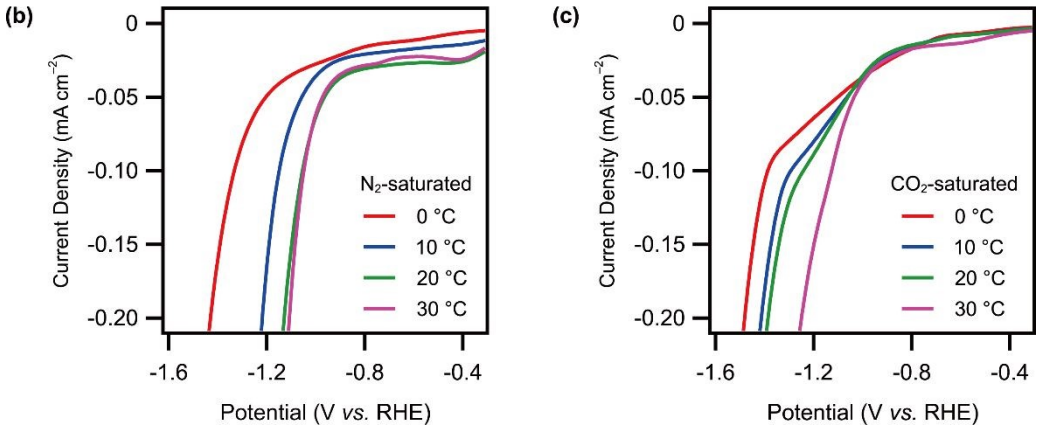

Fig. 5 Effect of the electrolyte temperature on the eCO_2RR performance. (a) Temperature dependence on the FEs for the eCO_2RR products at an applied potential of −1.46 V (*vs.* RHE), in 0.1 M $KClO_4$ aqueous solution, and at an electrolyte flow rate of 500 mL min^{-1}. (b, c) Linear sweep voltammograms in a 0.1 M $KClO_4$ aqueous solution saturated with N_2 (b) and CO_2 (c) potential range: 0.94 to −2.06 V (*vs.* Ag/AgCl); scan rate of 50 mV s^{-1}).

To assess the contribution of increased CO_2 solubility, we estimated the CO_2 solubility at each experimental temperature using the expression of Weiss.[24] The solubility increases from 29.8 mM at 30 °C to 36.9 mM at 22 °C, 48.5 mM at 13 °C, and 64.1 mM at 5 °C, corresponding to relative increases of 1.24-, 1.63-, and 2.15-fold relative to 30 °C. Comparing these values with the observed FE_{CO} (53% at 30 °C, 63% at 22 °C, 72% at both 13 °C and 5 °C) shows that the solubility increase alone does not quantitatively account for the full improvement in FE_{CO}, particularly at the lowest temperatures where FE_{CO} plateaus while solubility continues to rise. These observations suggest that increased CO_2 solubility and HER suppression act as concurrent factors, with the role of HER suppression becoming more pronounced at lower temperatures. We also acknowledge that local pH effects arising from OH^- accumulation near the electrode surface may contribute to the overall picture, and this warrants further investigation.

Integrated view of mass transport, interfacial microenvironment, and HER suppression

The flow-rate and temperature dependencies summarised above deserve to be considered together, because both primarily act on the same interfacial region probed by the analyses of Fig. 4. Increasing the electrolyte flow rate monotonically thinned the hydrodynamic diffusion layer, as quantified from chronoamperometry in $K_3[Fe(CN)_6]$ solution. One might expect that this would enhance the supply of all species participating at the interface, including protons, and therefore accelerate the competing HER as well as the eCO_2RR. However, FE_{H2} clearly decreased with increasing flow rate (Fig. 3), indicating that the two reactions are not

View Article Online
DOI: 10.1039/D6FD00071A

limited by the transport of the same species. In a dilute, weakly buffered $KClO_4$ electrolyte, HER on BDD is primarily fed by the reduction of water rather than of bulk H^+, and the associated local production of OH^- raises the near-surface pH. Enhanced convection continually refreshes the boundary layer with CO_2-saturated bulk electrolyte and simultaneously removes accumulated OH^-, so that the local concentration of dissolved CO_2 at the interface rises relative to that of water-derived protons. The net effect is a shift of the selectivity balance toward CO_2 reduction products, consistent with the simultaneous increase of FE_{CO} and suppression of FE_{H2} observed above 100 mL min^{-1}.

The temperature dependence provides independent support for this interpretation. The LSV experiments in CO_2-saturated $KClO_4$ (Fig. 5b, c) show that the apparent onset potential for HER shifts substantially toward more negative values as the temperature is lowered, whereas the onset potential associated with CO_2 reduction is essentially insensitive to temperature within the range investigated. This contrasting temperature sensitivity of the two competing reactions is noteworthy because, on metallic catalysts such as Au, Rodriguez and co-workers reported[26] that both onset potentials move in opposite but comparable directions, so that low temperature enhances selectivity mainly via a combined positive shift of the CO_2RR onset and a negative shift of the HER onset. The behaviour observed here on BDD is qualitatively different. The CO_2RR onset does not shift appreciably, and the improvement in FE_{CO} with decreasing temperature is consistent with HER suppression playing a significant role, alongside a concurrent increase in CO_2 solubility at lower temperatures. We note, however, that the onset potential criteria employed are operationally defined, and that a full mechanistic deconvolution of the solubility, kinetic, and local pH contributions would require additional experiments beyond the scope of the present study. A plausible origin of this contrast is the weak, essentially outer-sphere character of intermediate adsorption on the sp^3-carbon surface of BDD. With no strongly chemisorbed CO_2 activation pathway that would be thermally activated, the CO_2RR onset on BDD may be governed primarily by weakly interacting or outer-sphere-like electron transfer to CO_2,[27,28] which would be expected to exhibit only limited temperature dependence over a narrow range. In contrast, the HER on BDD is known to proceed with a large overpotential and significant thermal activation, which accounts for its pronounced sensitivity to the electrolyte temperature. The combined control of flow rate and temperature thus provides a straightforward route to enhancing FE_{CO} without invoking any modification of the BDD surface itself.

From the perspective of sustainable chemistry of electrofuels, it is useful to translate the optimised performance into the quantities relevant to an electrolyser stack. At the maximum Faradaic efficiency for CO of 72% reached at–1.46 V *vs.* RHE, 500 mL min^{-1}, and 5 °C, the corresponding j_{Total}, j_{CO}, and electrolysis time are summarised in Table S3. Essentially, all of the remaining charge is accounted for by HCOOH and H_2, both of which are valuable molecular energy carriers, and no carbon-containing by-products requiring energy-intensive separation are generated. The gas-phase output is a mixture of CO and H_2 that is in principle directly usable as syngas for Fischer–Tropsch or methanol synthesis without further purification.

Several limitations must, however, be explicitly acknowledged before drawing conclusions regarding PtX relevance. First, the partial current densities achieved in the present flow-cell geometry remain well below those of state-of-the-art Au- or Ag-based gas-diffusion electrode systems, and scaling to industrially relevant current densities will require migration to a gas-diffusion electrode or membrane-electrode-assembly configuration. Second, the full cell voltage was not independently measured in the present study, and energy efficiency values cannot therefore be reported at this stage; this represents an important parameter to be addressed in future work. Third, operating at 5 °C implies a thermal management load that would have to be carefully considered in the context of a scaled-up system. These considerations define the parameters, namely partial current density, energy efficiency, and thermal integration, that any realistic implementation of BDD-based PtX technology will need to address, and they are identified here as priorities for future investigation.

Conclusions

In summary, the present work advances on BDD electrodes along two complementary lines. First, the molecular modification results from our previous studies on aniline- and pyrazole-functionalised BDD are presented within a unified framework to establish that introducing nitrogen-based active sites effectively captures CO_2 and redirects the selectivity toward CO, and to motivate the development of a more practically accessible strategy. This recognition leads directly to the second and primary contribution of the present work: a systematic investigation of electrolyte engineering using $KClO_4$ aqueous solution, which achieves the same selectivity switch through a considerably more facile route.

Through a full parametric optimisation across applied potential, electrolyte flow rate, and operating temperature, we achieved a maximum FE_{CO} of 72% in 0.1 M $KClO_4$ aqueous solution at a potential of −1.46 V *vs.* RHE, a flow rate of 500 mL min^{-1}, and a temperature of 5 °C. The mechanistic analysis accompanying this optimisation yields two findings that are reported here for the first time. The flow-rate dependence is quantitatively accounted for by diffusion layer thinning, as confirmed by chronoamperometric measurements with a $[Fe(CN)_6]^{3-}$ redox probe, although we note that these measurements serve as a hydrodynamic proxy rather than a direct measure of the CO_2 concentration profile at the reacting BDD interface. More significantly, temperature-dependent LSV experiments reveal that, on BDD, the CO_2 reduction onset potential is essentially insensitive to temperature, whereas the HER onset shifts markedly negative upon cooling. This finding, namely that the improvement in FECO

at lower temperatures is consistent with HER suppression playing a significant role alongside a concurrent increase in CO_2 solubility, is qualitatively distinct from that reported on metallic catalysts and constitutes a new mechanistic insight into the eCO_2RR on sp^3-carbon surfaces.

View Article Online
DOI: 10.1039/D6FD00071A

Taken together, these findings establish the mechanistic foundations for redirecting eCO_2RR selectivity on BDD, and identify directions for its development as a metal-free platform for CO_2 conversion. Looking ahead, several directions emerge from the findings presented here. A first priority is to raise the partial current density for CO on BDD to levels compatible with an industrial PtX electrolyser, which will likely require migration from the present flow cell geometry to a gas-diffusion electrode or membrane-electrode-assembly configuration in which CO_2 is delivered directly to a porous BDD-based cathode. While the interfacial strategies described here, namely N-functionalisation and perchlorate-based electrolytes, are in principle applicable to such architectures, demonstrating their effectiveness in those configurations, together with measurement of full cell voltage and energy efficiency, remains an important objective for future work. A second direction concerns long-term stability under realistic, dynamic operation: our previous work has established that BDD itself is exceptionally durable, but data on how surface-anchored aniline or pyrazole layers survive repeated potential cycling and current interruptions typical of intermittent renewable power are still limited and deserve systematic investigation. Third, a further avenue is the coupling of selective CO production on BDD with simultaneous anodic valorisation of biomass-derived substrates, leading to paired co-electrolysis schemes that better match the energy and material flows of a net-zero chemical plant. Realising this potential at scale will, however, require addressing the engineering challenges identified above, namely electrode fabrication cost, operating overpotential, energy efficiency, and thermal management, which we hope the present mechanistic framework will help to navigate.

Data availability

The data supporting this article have been included as part of the Supplementary Information.

Author contributions

Takashi Yamamoto: Conceptualisation, Funding acquisition, Project administration (equal), Supervision (equal), Writing – original draft. **Taiga Ozawa:** Data curation, Formal analysis (lead), Investigation (equal). **Mai Tomisaki:** Formal analysis, Investigation (equal), Validation. **Yasuaki Einaga:** Funding acquisition (lead), Project administration (equal), Supervision (equal), Writing – review & editing.

Conflicts of interest

There are no conflicts to declare.

Acknowledgements

This work was partially supported by the JSPS Grant-in-Aid for Scientific Research A 23H00288, the New Energy and Industrial Technology Development Organisation (NEDO) P16002, and the Japan Science and Technology (JST) Agency CREST PMJCR24R7.

Notes and references

1 J. Artz, T. E. Muller, K. Thenert, J. Kleinekorte, R. Meys, A. Sternberg, A. Bardow and W. Leitner, *Chem. Rev.*, 2018, **118**, 434–504.
2 Q. Liu, L. Wu, R. Jackstell and M. Beller, *Nat. Commun.*, 2015, **6**, 5933.
3 H. Kumagai, Y. Tamaki and O. Ishitani, *Acc. Chem. Res.*, 2022, **55**, 978–990.
4 Y. Y. Birdja, E. Pérez-Gallent, M. C. Figueiredo, A. J. Göttle, F. Calle-Vallejo and M. T. M. Koper, *Nat. Energy*, 2019, **4**, 732–745.
5 S. Jin, Z. Hao, K. Zhang, Z. Yan and J. Chen, *Angew. Chem. Int. Ed.*, 2021, **60**, 20627–20648.
6 M. E. Dry, *Catal. Today*, 2002, **71**, 227–241.
7 P. De Luna, C. Hahn, D. Higgins, S. A. Jaffer, T. F. Jaramillo and E. H. Sargent, *Science*, 2019, **364**, eaav3506.
8 N. Yang, S. Yu, J. V. Macpherson, Y. Einaga, H. Zhao, G. Zhao, G. M. Swain and X. Jiang, *Chem. Soc. Rev.*, 2019, **48**, 157–204.
9 K. Natsui, H. Iwakawa, N. Ikemiya, K. Nakata and Y. Einaga, *Angew. Chem. Int. Ed.*, 2018, **57**, 2639–2643.
10 Z. J. Schiffer and K. Manthiram, *Joule*, 2017, **1**, 10–14.
11 O. S. Bushuyev, P. De Luna, C. T. Dinh, L. Tao, G. Saur, J. van de Lagemaat, S. O. Kelley and E. H. Sargent, *Joule*, 2018, **2**, 825–832.
12 A. Goeppert, M. Czaun, J. P. Jones, G. K. Surya Prakash and G. A. Olah, *Chem. Soc. Rev.*, 2014, **43**, 7995–8048.
13 T. Mikami, T. Yamamoto, M. Tomisaki and Y. Einaga, *ACS Sustainable Chem. Eng.*, 2022, **10**, 14685–14692.
14 E. Oh, Y. Einaga and T. Yamamoto, *ChemElectroChem*, 2026, **13**, e202500481.
15 M. Tomisaki, S. Kasahara, K. Natsui, N. Ikemiya and Y. Einaga, *J. Am. Chem. Soc.*, 2019, **141**, 7414–7420.
16 K. Natsui, T. Yamamoto, T. Watanabe, Y. Kamihara and Y. Einaga, *Phys. Status Solidi B*, 2013, **250**, 1943–1949.
17 M. Tomisaki, K. Natsui, N. Ikemiya, K. Nakata and Y. Einaga, *ChemistrySelect*, 2018, **3**, 10209–10213.

18 A. J. Bard and L. R. Faulkner, *Electrochemical Methods: Fundamentals and Applications, 2nd ed.*, Wiley, New York, 2001.
19 V. D. Brandão, H. Song, A. Venkataraman, Y. Fishler, S. S. Arora, S. S. Bhargava, C. Villa, A. Holewinski, S. Nair, M. C. Hatzell and C. Sievers, *ACS Catal.*, 2025, **15**, 8979–8990.
View Article Online
DOI: 10.1039/D6FD00071A
20 Y. Hori, H. Wakebe, T. Tsukamoto and O. Koga, *Electrochim. Acta*, 1994, **39**, 1833–1839.
21 R. I. Masel, Z. Liu, H. Yang, J. J. Kaczur, D. Carrillo, S. Ren, D. Salvatore and C. P. Berlinguette, *Nat. Nanotechnol.*, 2021, **16**, 118–128.
22 M. Farmand, A. T. Landers, J. C. Lin, J. T. Feaster, J. W. Beeman, Y. Ye, E. L. Clark, D. Higgins, J. Yano, R. C. Davis, A. Mehta, T. F. Jaramillo, C. Hahn and W. S. Drisdell, *Phys. Chem. Chem. Phys.*, 2019, **21**, 5402–5408.
23 L. W. Diamond and N. N. Akinfiev, *Fluid Phase Equilib.*, 2003, **208**, 265–290.
24 R. F. Weiss, *Mar. Chem.*, 1974, **2**, 203–215.
25 Y. Zong, P. Chakthranont and J. Suntivich, *J. Electrochem. Energy Convers. Storage*, 2020, **17**, 041007.
26 E. Sargeant, A. Kolodziej, C. S. Le Duff and P. Rodriguez, *ACS Catal.*, 2020, **10**, 7464–7474.
27 H. V. Patten, K. E. Meadows, L. A. Hutton, J. G. Iacobini, D. Battistel, K. McKelvey, A. W. Colburn, M. E. Newton, J. V. Macpherson and P. R. Unwin, *Angew. Chem. Int. Ed.*, 2012, **51**, 7002–7006.
28 I. Duo, C. Levy-Clément, A. Fujishima and C. Comninellis, *J. Appl. Electrochem.*, 2004, **34**, 935–943.

View Article Online
DOI: 10.1039/D6FD00071A

Data Availability Statement

The data supporting this article have been included as part of the Supplementary Information.